CrystEngComm

Accepted Manuscript

ROYAL SOCIETY OF CHEMISTRY

www.rsc.org/crystengcomm

Cite this: DOI: 10.1039/c0xx00000x

www.rsc.org/xxxxxx

ARTICLE TYPE

Synthesis of AgCl Hollow Cubes and Its Application in Photocatalytic Degradation of Organic Pollutants

Shikui Wu,[a,c] Xiaoping Shen,*[a,b] Zhenyuan Ji,[b] Guoxing Zhu[b] Chaojun Chen,[c] Kangmin Chen[a] Ren Bu,[c] and Limin Yang[c]

Received (in XXX, XXX) Xth XXXXXXXXX 20XX, Accepted Xth XXXXXXXXX 20XX
DOI: 10.1039/b000000x

A cuboidal AgCl hollow nanostructure has been synthesized by a simple one-pot reaction with $AgNO_3$ and CCl_4 as precursors. The synthesized product is characterized by X-ray diffraction, field emission scanning electron microscopy and transmission electron microscopy. The AgCl product consists of well-dispersed hollow cubes with a side length of 600-900 nm and a cavity size of 400-600 nm. The formation mechanism is investigated, and it is revealed that the growth of the hollow cubes involves a dissolution-precipitation process accompanied by ion diffusion. Light irradiation of the AgCl product causes the formation of plasmonic Ag/AgCl photocatalyst, which exhibits excellent photocatalytic activity for the degradation of organic contaminant of methyl orange (MO).

Introduction

Considering the localized surface plasmon resonance (LSPR) of noble metal nanoparticles and the good photosensitivity of silver halides, Ag/AgCl has been proposed as a new visible light plasmonic photocatalyst.[1] Several groups[2-4] have reported efficient and stable Ag/AgCl plasmonic photocatalysts with different morphologies such as pseudo-spherical,[5] cubic and semi-cubic AgCl micro-crystals,[6-11] Ag/AgCl nanowires,[12, 13] and AgCl crystals with exposed highly active facets.[14, 15] However, most of the reported synthetic procedures are multistep and time-consuming, and the morphology of the Ag/AgCl products is not well controlled due to the high reaction rate between the Ag^+ and Cl^- ions.[16, 17]

Materials with hollow and/or porous structures have larger specific surface area as compared to their solid counterparts, which enables them more applicable for catalysis, adsorption and drug-delivery.[18-20] Up to now, thermodynamically unfavorable hollow particles have been synthesized by using various strategy such as the nanoscale Kirkendall effect,[21-24] and ion exchange of inorganic solids.[25-27] However, AgCl hollow nanostructures have rarely been studied so far.[2] Recently, Tang *et al*. developed an interesting water soluble sacrificial salt-crystal-template (SCT) approach to Ag@AgCl cubic cages, which showed excellent photocatalytic activity towards the degradation of methyl orange (MO) due to their unique hollow structures. In this paper, we present a new and facile one-pot approach to prepare AgCl hollow cubic nanostructures using $AgNO_3$ and CCl_4 as silver and chlorine sources, respectively. Although AgCl hollow nanostructures have been prepared, to the best of our knowledge, this is the first report on hollow AgCl nanocubes prepared in one-pot by a solvothermal technique. A mechanism of dissolution-precipitation[28, 29] accompanied by ion diffusion is suggested for the formation of the hollow nanostructure. Furthermore, the Ag/AgCl plasmonic photocatalyst obtained by light irradiation of the AgCl hollow nanostructure exhibits excellent photocatalytic activity for organic contaminant degradation.

Materials and Methods

Materials:

All of the chemical reagents used in our experiments are of analytical grade, purchased from Sinopharm Chemical Reagent Co., Ltd, and used without further purification. Deionized water was used in all the experiments.

Synthesis of AgCl Hollow Nanocubes

In this synthesis, $AgNO_3$ and CCl_4 were used as silver and chlorine sources, respectively. Typically, 30 mg of $AgNO_3$ and 200 mg of PVP were dissolved in 40 mL of ethanol. Then, a solution of 8 mg of NaOH in 20 mL ethanol was added under magnetic stirring until a dark red solution (containing Ag seeds for the AgCl synthesis) was obtained. Subsequently, 12 mL of the dark red solution and 10 mL of CCl_4 were added into a 25 mL of Teflon-line stainless steel autoclave, sealed and maintained at 93 °C for 4 h. After the autoclave was cooled down to room temperature naturally, the AgCl product was collected by centrifugation, washed with ethanol and distilled water for five times, respectively, and dried at 45 °C in vacuum. The obtained sample was kept in dark for further characterization. For preparing Ag/AgCl plasmonic photocatalyst, the AgCl sample was dispersed in 10 mL water and irradiated with a 500 W tungsten lamp for *ca*. 10 min (Ag/AgCl-1), 20 min (Ag/AgCl-2), and 30 min (Ag/AgCl-3).

Instruments and characterization

The phase structures of the as-prepared products were characterized using powder X-ray diffraction (XRD, Rigaku D/MAX 2400) with Cu-K_α radiation (λ = 1.5406 Å) at a scanning rate of 2 º/min. The size, morphology and microstructure of the samples were characterized by field emission scanning electron microscopy (FESEM, Hitachi S-4800, with an accelerating voltage of 20 kV) and transmission electron microscopy (TEM, JEM-2100, with an accelerating voltage of 200 kV). Ultraviolet-visible (UV-vis) spectroscopy measurements were performed with a UV-2450 UV-vis spectrophotometer.

Photocatalytic measurements

The photocatalytic activities of the samples were evaluated by the degradation of methyl orange (MO) under a 500 W tungsten lamp irradiation. The tungsten lamp was positioned at *ca.* 10 cm away from the reaction cell to trigger the photocatalytic reaction. There is a water layer between the reaction system and the lamp to remove the thermal effect of light. The experiments were performed at room temperature as follows: 50 mg of the photocatalyst was added to 100 mL of MO solution (10 mg·L^{-1}) in a Pyrex reactor. Before illumination, the suspension was stirred in the dark for 30 min to ensure the establishment of an adsorption-desorption equilibrium between the photocatalyst and MO. The dispersion was then exposed to the light irradiation under stirring. At given time intervals, 4 mL of the suspension was pipetted into a centrifuge tube and centrifuged at 8000 rpm for 2 min to remove the remnant photocatalyst. The concentrations of MO in the supernatant were monitored by checking the absorbance at 664 nm using the UV-vis spectrophotometer. Total organic carbon (TOC) was measured using a TOC analyzer (Analytik Jena AG multi N/C 2100)

Results and Discussion

Structural and morphological characterization

Figure 1a shows the XRD pattern of as-synthesized AgCl product. All of the diffraction peaks are consistent with the standard XRD data of the cubic-phase AgCl (JCPDS No: 31-1238). No other peaks from impurity could be observed, revealing the pure AgCl product. Figure 1b presents a representative FESEM image of the AgCl hollow nanostructures, which clearly indicates that the product is composed of a large quantity of regular cube-like crystals with a hollow cavity in the centre of each cube. From the high magnification FESEM image (Figure 1c and 1d), it can be seen that the side length of the cubes is about 600-900 nm. Some cubes become so hollow that the walls of the cubes are broken forming cube-like frame structures (Figure 1d). The hollow nanostructures of the as-synthesized AgCl were further revealed by TEM. A strong contrast difference in the cube-like crystals with a bright center surrounded by a much darker edge confirms their hollow architecture (Figures 1e and 1f). The wall-thickness of the hollow cubes is usually less than 100 nm and the size of the cavity is about 400-600 nm. Under the irradiation of electron beams, some irregular Ag nanoparticles can be observed on the surface of hollow cubes.

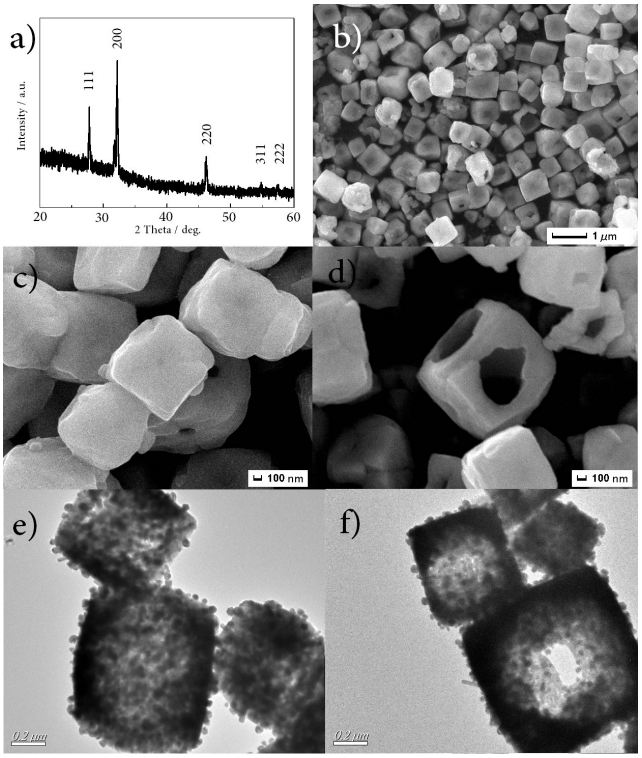

Figure 1. (a) XRD pattern, (b, c, d) FESEM and (e, f) TEM images of the as-prepared AgCl hollow cubes.

Formation process of AgCl hollow cubes

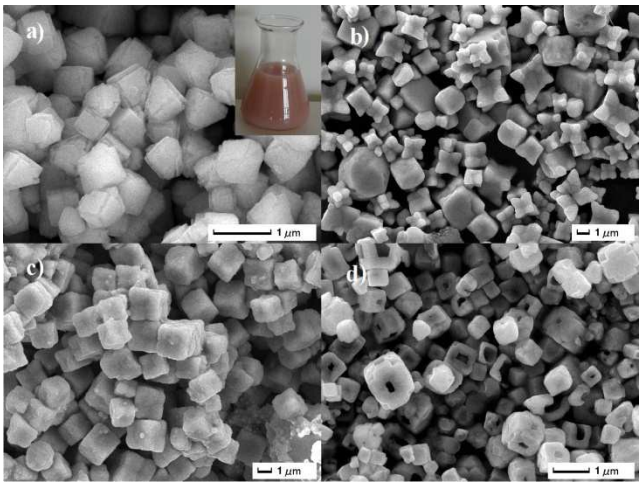

Figure 2. FESEM images of the products synthesized with different solvothermal reaction time: a) 1 h, b) 2 h, c) 3 h, d) 4.5 h.

The growth of the AgCl hollow cubes was then carefully investigated by analysing the products obtained with different reaction time. First, the $AgNO_3$ was transformed into Ag_2O under alkaline condition, which was easily reduced to Ag^0 seeds by ethanol. As a result, a dark red dispersion was obtained (Fig. S1a). XRD pattern of the as-formed Ag seeds can be indexed to cubic-phase metallic silver (JCPDS No: 65-2871) (Figure S2a). TEM and HRTEM images of Ag seeds were shown in Figure S3. The Ag seeds show quasi-spherical shape with relatively small size. The fringe spacing of 2.36 Å observed in Figure S3b can be indexed to the {111} planes of face-centered cubic (fcc) Ag.

After 1 hour reaction of the Ag^0 seeds with CCl_4, the dark red dispersion was turned into a reddish one. The corresponding FESEM image was shown in Figure 2a. It can be seen that the Ag cores are covered by a new shell layer. XRD pattern of the reddish sample exhibits that besides two weak peaks at $2\theta = 38.1°$ (111) and 44.3° (200) originated from metallic Ag, the main diffraction peaks can be indexed to the cubic phase AgCl (Fig. S2b). These results suggested that AgCl was generated on the Ag^0 seed.[30] As the reaction time increases, the products become flower-like morphology at 2 h (Fig. 2b) and pseudo-cubic one at 3 h (Fig. 2c) with an increasing uniformity of particle size. As shown in Figure 2b and 2c, the cranny on the surface of the particles is convinced of the grown vestige. Due to the instability of AgCl under the strong irradiation of electron beams, HRTEM image of AgCl cannot be obtained. Therefore, the growth of the AgCl crystals is investigated by geometry based on its simple cubic structure.[31] The regular AgCl hollow cubes were obtained after 4 h reaction (Figure 1b). If further prolonging the reaction time, the hole in the cubes will become larger, that is the reason why more microframes can be obtained at 4.5 h (Figure 2d).

Possible formation mechanism of the AgCl hollow cubes

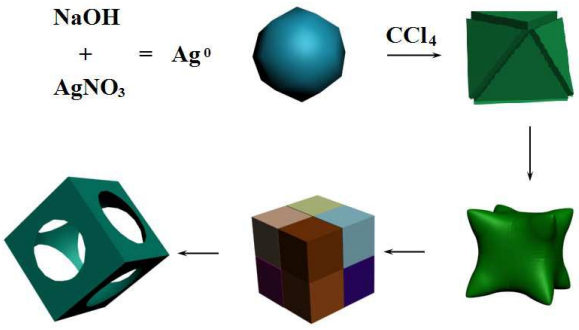

Scheme 1. The formation process of AgCl hollow cubes.

Based on the above results, the formation mechanism of the AgCl hollow cubes is suggested to involve a three-step process as shown in Scheme 1.

(1) Formation of metallic Ag seeds:

As shown above, Ag seeds were firstly generated in the presence of $AgNO_3$ and NaOH in ethanol solution. Here, ethanol acts as a reducing agent,[32] in accord with the spontaneous reduction of silver ions to Ag particles in NaOH 2-propanol solution. [33]

$$2Ag^+ + 2OH^- \longrightarrow Ag_2O + H_2O$$

$$C_2H_5OH + Ag_2O \xrightarrow{OH^-} CH_3CHO + 2Ag^0 + H_2O$$

Meanwhile, Ag_2O and Ag^+ can also be reduced to Ag^0 by CH_3CHO.

$$CH_3CHO + 2Ag^+ + 2OH^- \longrightarrow CH_3COOH + 2Ag^0 + H_2O$$

$$CH_3CHO + Ag_2O \xrightarrow{OH^-} CH_3COOH + 2Ag^0$$

(2) Formation of AgCl on the {111} facets of Ag particles. [34]

$$(4\text{-}x)\ Ag + CCl_4 \rightarrow (4\text{-}x)\ AgCl + CCl_x$$

The net free energy change ($\Delta_r G^0$) for the reaction is -374.0 $kJ \cdot mol^{-1}$ when $x = 0$. The reaction is feasible in theory, but it is a slow process in ambient condition. [35]

In solvothermal condition, the quasi-sphere shaped Ag^0 seeds have a tendency to aggregate.[36] When heated, the Ag^0 seeds aggregated to form bigger nanoparticles to minimize the surface energy.[37] Then, a layer of AgCl was *in-situ* produced on the surface of Ag nanoparticles. With the proceeding of the reaction, Ag nanoparticles could evolve into octahedral particles. [38]

(3) A dissolution-precipitation process occurs: some little granules were 'eaten' by the regular larger particles, which is why regular flowers and cubes can be obtained in different reaction time. Meanwhile, the Ag atoms in the core of cubes gradually diffuse outward, and react with CCl_4 on the surface, where Ag atoms could be oxidized by CCl_4 to form AgCl and deposited on the surface of each cube as a shell. So far, many cases have proved that cation diffusion is much faster than anion diffusion. [22, 24] In this case Ag cations or atoms diffuse faster than incoming Cl species, which cause a void space inside the cube, and leads to the formation of a hollow structure. This is why a series of morphologies can be obtained just by adjusting the reaction time.

Photocatalytic activity of the Ag/AgCl hollow cubes

Atomic composition analysis (Table S1) confirmed that the Ag:AgCl ratio could be tailored by varying the light irradiation time. The results show that with increasing irradiation time, the surface of the AgCl nanocubes gradually reduced to metallic Ag. The best photocatalytic performance was observed at an Ag:AgCl molar ratio of 9.6:100 (Ag/AgCl-2). However, the interface between the AgCl and Ag is enlarged on further increasing the Ag content, thereby increasing hole capture by the negative surface charge on the Ag nanograins, which may reduce the efficiency of charge separation. This may account for the lower photocatalytic activity of Ag/AgCl-3.[39, 40]

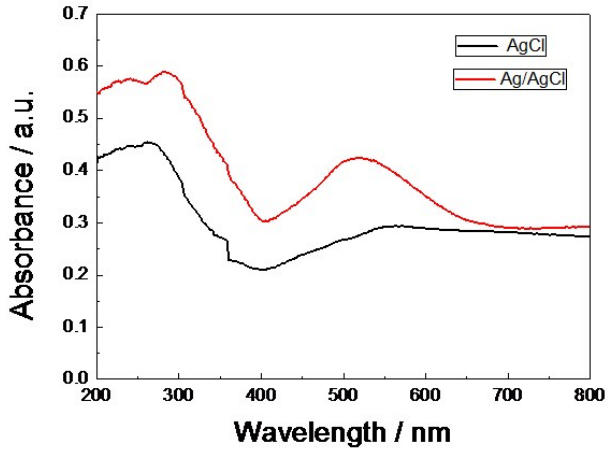

Figure 3. UV-vis diffuse reflectance spectra of AgCl and Ag/AgCl-1 hollow cubes.

It is well known that optical absorption plays an important role in determining the photocatalytic performance of a catalyst, especially in the photodegradation of organic pollutants.[41, 42] Sunlight energized catalysts are highly expected due to the higher efficiency and the effective utilization of sun energy. The optical properties of bare AgCl and Ag/AgCl hollow nanostructures were probed by UV-vis diffuse reflectance spectroscopy (Figure 3). For AgCl cubes, the absorption is mainly observed in the UV region, only with a negligible absorption in the visible region. In contrast, the as-prepared Ag/AgCl-1 sample exhibits a broad absorption band at *ca.* 400-650 nm besides the UV absorption similar to the pure AgCl cubes. The absorption at 400-650 nm

could be ascribed to the characteristic LSPR absorption of the Ag nanoparticles on the surface of AgCl.

The photocatalytic activity of the as-synthesized products was then investigated with degradation of MO under tungsten lamp irradiation as a model reaction. The commercial nitrogen-doped TiO_2 (T_{25}) photocatalyst was also used for comparison. As shown in Figure 4a, the photocatalytic performance increases in the order of T_{25}, bare AgCl, and Ag/AgCl. The T_{25} catalyst shows the poorest photodegradation activity, and the Ag/AgCl hollow cubes shows much enhanced photocatalytic activity compared to that of pristine AgCl hollow cubes. After irradiation for 30 min, only 50% of MO was removed over the pristine AgCl, while the removal ratio reaches 97% on the Ag/AgCl-2 hollow cubes. To evaluate the stability and reusability of the AgCl/Ag samples, we also performed a recyclability test involving repeated photodegradation of MO with AgCl/Ag-2. As shown in Figure 4b, after five cycles of the photodegradation of MO, the catalyst exhibits only a small loss of the activity, indicating its good stability for repeated photocatalysis.

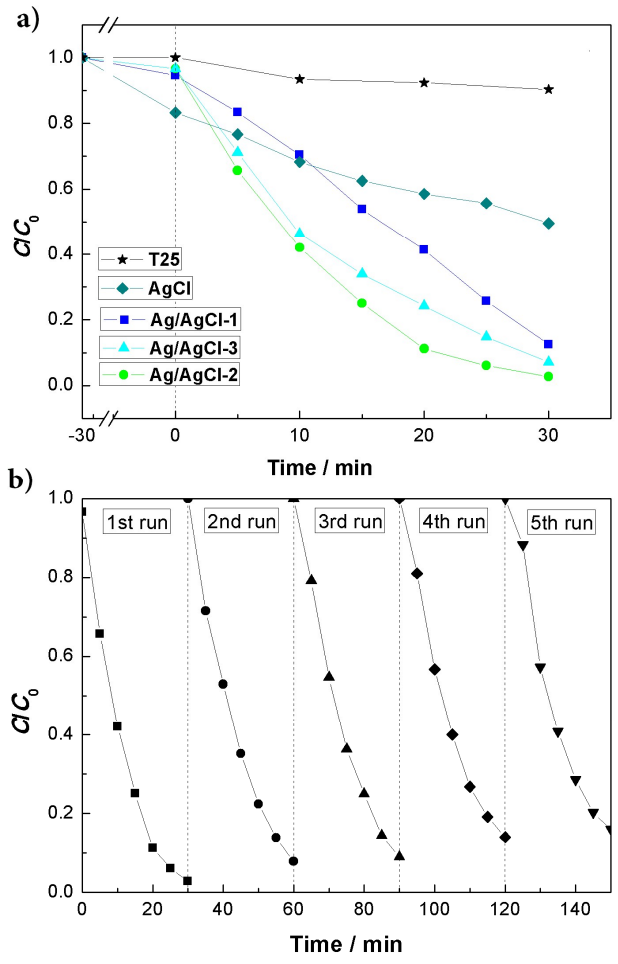

Figure 4. a) Photodegradation of MO with catalysts of T25, the as-prepared AgCl and Ag/AgCl hollow cubes under tungsten lamp irradiation. c_0 is the initial concentration of MO aqueous solution (10 mg·L^{-1}), and c is the instantaneous concentration of MO solution during photodegradation. b) Recycling test on the representative Ag/AgCl-2 for MO photodegradation.

TOC analysis confirmed that mineralization involved in this photocatalytic decomposition of MO.[43] Under tungsten lamp irradiation for 30 min, AgCl, Ag/AgCl-1, Ag/AgCl-2, and Ag/AgCl-3 exhibited the TOC loss value of 64, 74, 79 and 77% over pristine dye solution, suggesting that mineralization process engaged in the decomposition of MO. It further confirmed that Ag/AgCl-2 has the best photocatalytic activity. The decrease of TOC shows that MO can be completely photodegraded by the Ag/AgCl catalysts even though it takes more time than the process of decoloration.

The kinetics of the degradation reaction can be fitted to a pseudo-first-order reaction (Figure S4), and the rate constant can be obtained by the slope of the straight line. For the Ag/AgCl-2 hollow structure, the rate constant was estimated to be 0.1177 min^{-1}, which is bigger than that of the reported Ag/AgCl composites.[40] Furthermore, in order to compare the photocatalysis activities of our Ag/AgCl hollow cubes and the Ag@AgCl cubic cages reported by Tang *et al.*,[2] we measured the photocatalytic property of the AgCl/Ag-2 sample using a 250 W xenon lamp as the light source. The experimental results are shown in Figure S5. It can be seen that about 97% of MO was degraded over the Ag/AgCl-2 catalyst after only 10 min irradiation. Obviously, the photocatalytic activity of the Ag/AgCl hollow cubes is remarkably improved when using 250 W Xenon lamp instead of 500 W tungsten lamp as light source. This photocatalytic activity is comparable to the Tang's result, in which the degradation needs about 360 s (6 min) under the irradiation of a 300 W Xenon lamp.[2] This result further demonstrates that the hollow nanostructure can enhance the photocatalytic activity of Ag/AgCl. This is reasonable because for hollow nanostructure, more coordination sites on the unsaturated surface are exposed to the solution. [44-46] The reactant molecules can efficiently access the active sites, and hence enhance the photocatalytic efficiency [47, 48]

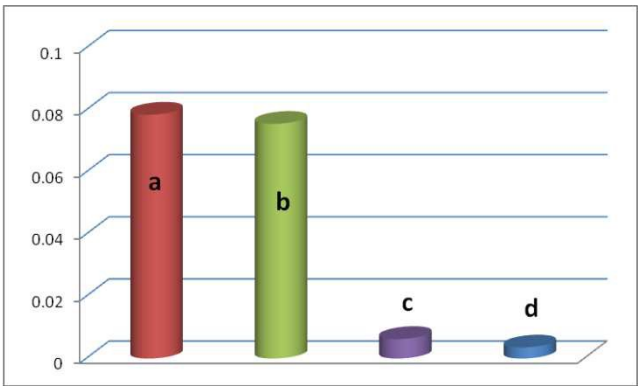

Figure 5. Kinetic rate constants of the Ag/AgCl-1 hollow cubes for the photodegradation of MO in the presence of hole and radical scavengers: (a) Ag/AgCl, (b) Ag/AgCl + 1 mM t-BuOH, (c) Ag/AgCl + 1 mM BZQ, and (d) Ag/AgCl + 1 mM TEOA.

The excellent photocatalytic activity of the synthesized hollow cubes motivated us to investigate the photocatalytic mechanism of the degradation process. It is well known that active species such as holes, hydroxyl radicals (·OH), and superoxide radicals ($O_2^{\cdot-}$) are usually involved in the photodegradation process.[49] To investigate the main active species and to gain further insight into the underlying photocatalytic mechanism, three different chemicals of triethanolamine (TEOA, a hole scavenger), *tert*-butyl alcohol (*t*-BuOH, a ·OH radical scavenger) and *p*-

benzoquinone (BZQ, a $O_2^{\cdot -}$ radical scavenger), were introduced in the reaction system.[50, 51] As shown in Figure 5, the rate constants for the Ag/AgCl nanostructures in the presence of *t*-BuOH, BZQ, and TEOA were estimated to be 0.0756, 0.0062, and 0.0035 min^{-1}, respectively. Therefore, the introduction of TEOA and BZQ caused a remarkable decrease in the photocatalytic degradation of MO, whereas the presence of *t*-BuOH had no deleterious effect on the photocatalytic activity. These results suggest that direct hole and $O_2^{\cdot -}$ radicals oxidation govern the photocatalytic process, and ·OH radical was not the main active oxidative species in the photocatalytic degradation of MO.

As shown above, pure AgCl can only absorb UV light because its direct and indirect bandgaps are 5.6 and 3.25 eV, respectively.[52] Therefore, the high photocatalytic activity under tungsten lamp irradiation should be ascribed to the contribution of Ag nanoparticles, which can absorb visible light by surface plasmon resonance.[1] Because of the synergy of the excellent conductivity of Ag nanoparticles and the polarization effect of negatively charged AgCl surface,[53] the photogenerated electrons are transferred to the surface of the Ag nanoparticles far from the Ag-AgCl interface. These photogenerated electrons together with the injected LSPR electrons were trapped by oxygen molecules (O_2) in the solution to form superoxide ions ($O_2^{\cdot -}$),[54] which oxidize the MO dye molecules. Meanwhile, the holes will combine with Cl^- ions to form Cl^0 atoms. Because of the high oxidation ability of the Cl^0 atoms, the MO dye could be oxidized by the Cl^0 atoms and hence the Cl^0 could be reduced to Cl^- ions again. [53] The possible process was briefly shown in Figure 6. In addition, because of the in situ production of Ag nanoparticles on the surface of AgCl, the well-defined interface facilitates the interfacial electron transfer and promotes carrier separation, which may make another contribution to the high photocatalytic activity.[13]

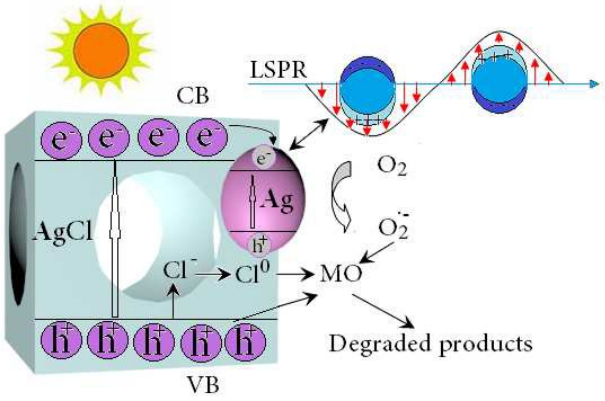

Figure 6. Proposed mechanism for the photocatalytic degradation of MO over Ag/AgCl hollow cubes under tungsten lamp irradiation.

Conclusions

In summary, we have developed a novel one-step solvothermal method for large-scale synthesis of AgCl hollow cubes. The morphology evolution process of AgCl nanostructures was detailedly investigated, and a possible formation mechanism for the AgCl hollow cubes is proposed. Light irradiation of the AgCl hollow cubes resulted in plasmonic Ag/AgCl photocatalyst, which show much enhanced photocatalytic performance compared to the pristine AgCl due to the SPR effect of the metallic silver. Meanwhile, the possible degradation mechanism of the Ag/AgCl plasmonic photocatalyst was also proposed. It is expected that the Ag/AgCl hollow cubic nanostructure would have potential application in the degradation of organic contaminations as well as in photovoltaic cells and other optoelectronic devices.

Acknowledgements

The authors are grateful for financial support from National Nature Science Foundation of China (No. 51272094), Doctoral Innovation Program Foundation of Jiangsu Province (KYLX_1026), Natural Science Foundation of Inner Mongolia (2012MS1209) and Young Foundation of Inner Mongolia Medical University(YKD2012QNCX020).

Notes and references

a. School of Material Science and Engineering, Jiangsu University, Zhenjiang 212013, P. R. China.
b. School of Chemistry and Chemical Engineering, Jiangsu University, Zhenjiang 212013, P. R. China. Tel/Fax: +86-511-88791800; E-mail:xiaopingshen@163.com.
c. Inner Mongolia Medical University, College of Pharmacy, Hohhot 010059, P. R. China. E-mail:shikuiwu@yahoo.com.

1 P. Wang, B. Huang, X. Qin, X. Zhang, Y. Dai, J. Wei, and M Whangbo. *Angew. Chem. Int. Ed.* 2008, **47**, 7931.
2 Y. Tang, Z. Jiang, G. Xing, A. Li, P. D. Kanhere, Y. Zhang, T. C. Sum, S. Li, X. Chen, Z. Dong and Z. Chen *Adv. Funct. Mater.* 2013, **23**, 2932.
3 P. Wang, B. Huang, Z. Lou, X. Zhang, X. Qin, Y. Dai, Z. Zheng and X. Wang. *Chem. Eur. J.* 2010, **16**, 538.
4 Y. Li, Y. Ding. *J. Phys. Chem. C*, 2010, **114**, 3175.
5 L. Kuai, B. Geng, X. Chen, Y. Zhao, and Y. Luo. *Langmuir*. 2010, **26**, 18723.
6 D .Chen, S. Yoo, Q. Huang, G. Ali and S. O. Cho. *Chem Eur J*. 2012, **18**, 5192.
8 H. Wang, X. Lang, J. Gao, J. Gao, W. Liu, D. Wu, Y. Wu, L. Guo and J. Li. *Chem Eur J*. 2012, **18**, 4620.
9 L. Han, P. Wang, C. Zhu, Y. Zhai and S. Dong. *Nanoscale*, 2011, **3**, 2931.
10 C. An, S. Peng, Y. Sun, *Adv. Mater.* 2010, **22**: 2570.
11 C. An, R. Wang, S. Wang, and X. Zhang. *J. Mater. Chem.*, 2011, **21**, 11532.
12 Y. Bi, J. Ye. *Chem. Commun*. 2009, **43**, 6551.
13 Y. Bi, J. Ye. *Chem. Eur. J* 2010, **16**, 10327.
14 G. Liu, J. Yu, G. Lu, *Chem Commun.* 2011, **47**, 6763.
15 M. Zhu, P. Chen, and M Liu. *J. Mater. Chem.*, 2012, **22**, 21487.
16 R. Dong, B. Tian, C. Zeng, T. Li, T. Wang, and J. Zhang. *J. Phys. Chem. C* 2013, **117**, 213.
17 Y. Li and Y. Ding. *J. Phys. Chem. C* 2010, **114**, 3175.
18 J. Zheng, X. Wang, W. Li. *CrystEngComm*, 2012, **14**, 7616.
19 H. Goesmann, C. Feldmann, *Angew. Chem. Int. Ed.* 2010, **49**, 1362.
20 G. Dong, Y. Zhu, *CrystEngComm*, 2012, **14**, 1805.
21 H. Fan, U. Gosele, M. Zacharias. *Small* 2007, **3**, 1660.
22 Y. Yin, R. Rioux, C. Erdonmez, S. Hughes, G. A. Somorjai, and A. P. Alivisatos. *Science* 2004, **304**, 711.
23 Y. Yin, C. K. Erdonmez, A. Cabot, S. Hughes and A. P. Alivisatos. *Adv. Funct. Mater.*2006, **16**, 1389.
24 Y. Wang, L.Cai, Y. Xia, *Adv. Mater.* 2005, 17: 473.
25 D. Son, S. Hughes, Y. Yin, and A. P. Alivisatos. *Science* 2004, **306**, 1009.
26 L. Dloczik, R. Konenkamp. *Nano Lett.* 2003, **3**, 651.

27 M. Kovalenko, D. Talapin, M. Loi, F. Cordella, G. Hesser, M. I. Bodnarchuk and W. Heiss. *Angew. Chem. Int. Ed.* 2008, **47**, 3029.
28 J. Park, H. Zheng, A. P. Alivisatos, *J. Am. Chem. Soc.*, 2009, **131**, 13943.
29 J. Eckert Jr., C. Hung-Houston, B. Gersten, M. M. Lencka and R. E. Riman. *J. Am. Ceram. Soc.*, 1996, **79**, 2929.
30 B. Cai, J. Wang, S. Gan, D. Han, Z. Wu and L. Niu. *J. Mater. Chem. A*, 2014, **2**, 5280.
31 Z. Lou, B. Huang, X. Qin, *Chem. Commun.*, 2012, **48**, 3488.
32 R. Brenier. *J. Phys. Chem. C* 2009, **113**, 1758.
33 Z. Y. Huang, G. Mills, B. Hajek. *J. Phys. Chem.* 1993, **97**, 11542.
34 K. Doll1, N. M. Harrison. *Phys. Rev. B* 2001, **63**, 165410.
35 M. S. Bootharaju, G. K. Deepesh, T. Udayabhaskararao, and T. Pradeep. *J. Mater. Chem. A*, 2013, **1**, 611.
36 M. Moskovits, B. Vlckova. *J. Phys. Chem. B*. 2005, **109**, 14755.
37 S. Wu, C. Chen, X. Shen, G. Li, L. Gao, A. Chen, J. Hou and X. Liang. *CrystEngComm*, 2013, **15**, 4162.
38 Y. Wang, D. Wan, S. Xie, X. Xia, C. Huang, and Y. Xia. *ACSnano*. 2013, **7**, 4586.
39 J. Jiang, L. Zhang. *Chem. Eur. J* 2011, 17: 3710.
40 H. Xu, H. Li, J. Xia, S. Yin, Z. Luo, L. Liu, and L. Xu. *Acs Appl. Mater. Inter*, 2011, 3: 22.
41 Y. Zhang, Z. Tang, X. Fu, and Y. Xu. *ACS Nano* 2010, **4**, 7303.
42 N. Zhang, Y. H. Zhang, Y. J. Xu, *Nanoscale* 2012, **4**, 5792.
43 M. Choi, K. Shin, J. Jang. *J. Colloid Interface Sci. 20*10, **341**: 83.
44 L. Ji, W. Chen, L. Duan. *Environ. Sci. Technol.* 2009, **43**, 2322.
45 P.H. Chang, Z.H. Li, T.L. Yu, S. Munkhbayer, T. Kuo, Y. Hung, J. Jean, K. Lin. *J. Hazard. Mater.* 2009, **165**, 148.
46 J. Kang, H. Liu, Y.M. Zheng, Jiuhui Qu, J. Paul Chen. *J. Colloid Interface Sci*. 2010, **354**, 261.
47 X. Zhang, Z. Ai, F. Jia, and L. Zhang. *J. Phys. Chem. C* 2008, **112**, 747.
48 X. Xiao, W.D. Zhang, *J. Mater. Chem.* 2010, **20**, 5866.
49 W. Li, D. Li, Y. Lin, P. Wang, W. Chen, X. Fu, and Y. Shao. *J. Phys. Chem. C* 2012, **116**, 3552.
50 X. F. Yang, H. Y. Cui, Y. Li, J. Qin, R. Zhang, and H. Tang. *ACS Catal.* 2013, **3**, 363.
51 G. Z. Liao, S. Chen, X. Quan, H. Yu and H. Zhao. *J. Mater. Chem.* 2012, **22**, 2721.
52 M. R. Hoffmann, S. T. Martin, W. Choi, D. W. Bahnemann. *Chem. Rev.* 1995, **95**, 69.
53 B. Tian, J. Zhang. *Catal Surv Asia,* 2012, **16**, 210.
54 S.S. Soni, M.J. Henderson, J.F. Bardeau, and A. Gibaud. *Adv. Mater.* 2008, **20**, 1493.

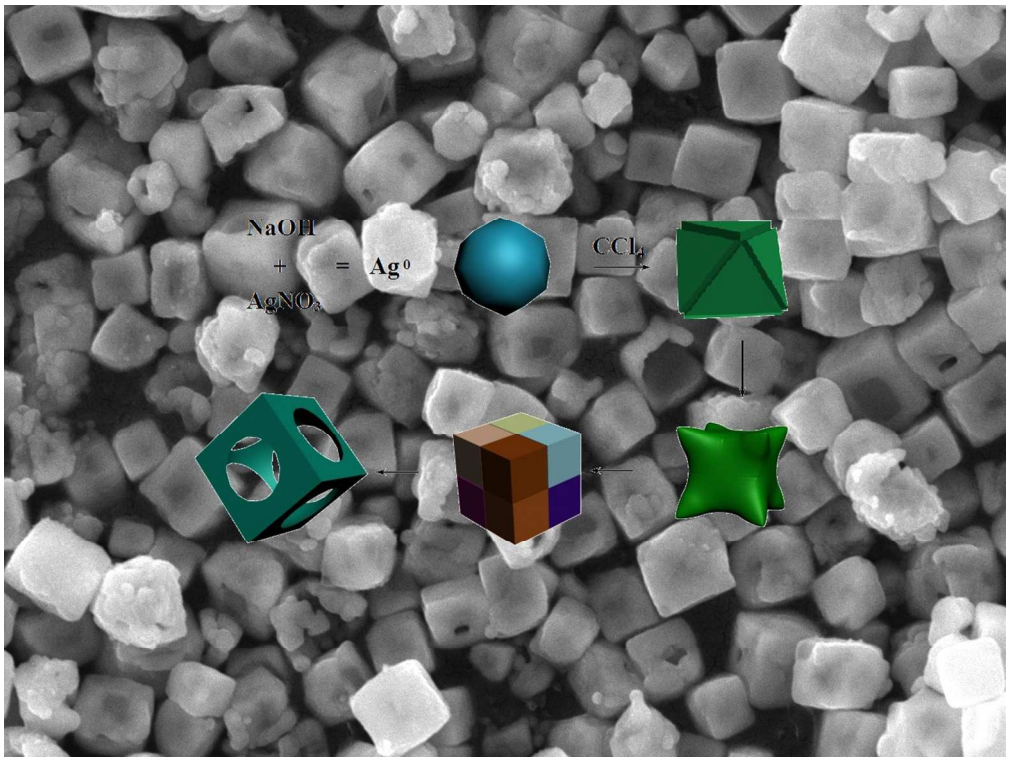

The formation process and typical FESEM image of AgCl hollow cubes
119x89mm (271 x 271 DPI)